

# Dielectric-Dependent Range-Separated Hybrid Functional Calculations for Metal Oxides

Jiawei Zhan,<sup>1</sup> Marco Govoni,<sup>1,2,3</sup> and Giulia Galli<sup>1,2,4,\*</sup>

<sup>1</sup>*Pritzker School of Molecular Engineering,*

*University of Chicago, Chicago, Illinois 60637, United States*

<sup>2</sup>*Materials Science Division and Center for Molecular Engineering,  
Argonne National Laboratory, Lemont, Illinois 60439, United States*

<sup>3</sup>*Department of Physics, Computer Science, and Mathematics,  
University of Modena and Reggio Emilia, Modena, 41125, Italy*

<sup>4</sup>*Department of Chemistry, University of Chicago,  
Chicago, Illinois 60637, United States*

(Dated: February 19, 2025)

## Abstract

Recently, we introduced the screened-exchange range-separated hybrid (SE-RSH) functional to account for spatially dependent dielectric screening in complex materials. The SE-RSH functional has shown good performance in predicting the electronic properties of a large variety of semiconductors and insulators, and of heterogeneous systems composed of building blocks with large dielectric mismatch. Here, we assess the performance of SE-RSH for oxide materials, including antiferromagnetic transition-metal oxides. Through a comparison with other dielectric-dependent hybrid functionals, we demonstrate that SE-RSH yields improved predictions of dielectric constants and band gaps, bringing them into a closer agreement with experimental values. The functional also provides accurate values of magnetic moments of several oxides.

## I. INTRODUCTION

Metal oxide semiconductors and insulators are versatile materials used in numerous applications, ranging from energy conversion and storage to environmental technologies[1–5]. The broad applicability of metal oxide (MO) semiconductors stems from their optoelectronic properties and the ability of metal cations to readily switch oxidation states under the presence of external fields, making MOs particularly valuable for redox and charge transfer reactions. These characteristics have positioned these materials at the forefront of research in sustainable energy sources, including solar-driven water splitting[6, 7], photovoltaics[8], and heterogeneous catalytic processes[9].

From a theoretical standpoint, the description of MOs relevant to energy conversion technologies poses several challenges. For example, the study of heterogeneous systems at the atomistic level, such as the interface between an oxide semiconductor and an electrolyte present in photoelectrochemical cells, often requires large supercells and advanced theoretical methods to describe light-matter interactions (e.g., many-body perturbation theory[10, 11] or time-dependent techniques). However, such approaches can be computationally prohibitive for large systems. Consequently, approximate strategies are often employed, where density functional theory (DFT) is used to treat solid and liquid phases separately, followed by an *a posteriori* description of their interaction[12–14].

---

\* gagalli@uchicago.edu

Even putting aside the complexities of materials heterogeneity, computing accurate properties of MOs using DFT remains challenging. Local and semi-local exchange and correlation energy functional (xc) functionals are known to severely underestimate the value of fundamental band gaps[15]. Hybrid functionals, in which the exchange energy is obtained as a linear combination of exact Hartree-Fock and local exchange energies, have emerged as a more accurate alternative to (semi)-local functionls, with PBE0[16] and HSE[17–19] being popular ones to describe condensed systems.

Among hybrid functionals, dielectric-dependent (DD) hybrid functionals[20–24], such as DD-RSH-CAM[25], RSH[20] and DDH[21], have been increasingly adopted to investigate the structural and electronic properties of pristine [22, 24] and defective[26] solids, liquids[27, 28] and also of several molecules[24]. For solids, this class of functionals is defined using the dielectric constant of the system. Despite the success of DD hybrid functionals in predicting the band gaps of many insulators and semiconductors, several studies[29, 30] have pointed at remaining inaccuracies for bulk metal oxides. Specifically, the DD-RSH-CAM functional tends to overestimate the band gaps of specific oxides, especially those of challenging antiferromagnetic transition-metal monoxides, MnO, CoO and NiO[25, 29]. Alternative approaches include Koopmans-compliant functionals[31–34] and related functionals based on the Wannier–Koopmans Method (WKM)[35–37], both of which reliably predict band gaps for main-group covalent semiconductors. However, the performance of WKM for the band gaps of transition metal oxides with partially filled d-states is not fully satisfactory[38].

Recently, we proposed the SE-RSH functional[39], designed to extend the applicability of dielectric-dependent hybrid functionals to complex heterogeneous systems. By explicitly incorporating a spatially dependent dielectric screening, SE-RSH can account for varying screening environments experienced by different electronic states, and can accurately describe both localized and delocalized states. Hence, SE-RSH is expected to capture the often mixed character of oxide materials’ band edges, to which both itinerant (arising from oxygen s and p orbitals) and localized (arising from metal cation d or f orbitals) states may contribute.

In this work, we provide a comprehensive validation of the performance of the SE-RSH functional for various metal oxides, focusing on band gaps, dielectric constants, and magnetic moments. We obtain results in good agreement with experiments for systems ranging from simple oxide, such as alumina to challenging antiferromagnetic systems, such as Co and Ni

oxides.

The remainder of this paper is organized as followed. In Section II, we revisit the expression of SE-RSH and highlight key differences from previous dielectric-dependent hybrid functionals. Section III presents electronic properties computed using SE-RSH, and Section IV summarizes our findings.

## II. METHOD

### A. General Hybrid Functionals for Complex Materials

When defining range-separated hybrid functionals[40–46], the non-local exchange potential  $v_x(\mathbf{r}, \mathbf{r}')$  that enters the Kohn-Sham (KS) Hamiltonian under the generalized Kohn-Sham scheme takes the form:

$$v_x(\mathbf{r}, \mathbf{r}') = \alpha(\mathbf{r}, \mathbf{r}')\Sigma_x(\mathbf{r}, \mathbf{r}') + (1 - \alpha_{lr})v_x^{lr}(\mathbf{r}; \mu) + (1 - \alpha_{sr})v_x^{sr}(\mathbf{r}; \mu), \quad (1)$$

where  $\Sigma_x$  represents the Hartree-Fock (exact) exchange, while  $v_x^{lr}$  and  $v_x^{sr}$  denote the long-range (lr) and short-range (sr) components of the semilocal exchange, respectively. The mixing fraction  $\alpha(\mathbf{r}, \mathbf{r}')$  controlling the combination of exact and semilocal exchange is given by:

$$\alpha(\mathbf{r}, \mathbf{r}') = \alpha_{lr} + (\alpha_{sr} - \alpha_{lr})\text{erfc}(\mu|\mathbf{r} - \mathbf{r}'|), \quad (2)$$

where  $\alpha_{lr}$  and  $\alpha_{sr}$  determine the fraction of exact exchange in the lr and sr components, respectively, and  $\mu$  is a screening parameter.

Recently, range-separated dielectric-dependent hybrid functionals (RS-DDH)[20, 23, 25] have been proposed, that yield accurate electronic properties of inorganic materials and molecular crystals by relating the parameters entering  $\alpha(\mathbf{r}, \mathbf{r}')$  to system-dependent dielectric properties. Specifically, in RS-DDH,  $\alpha_{lr}$  is set to the inverse of the macroscopic dielectric constant  $\varepsilon_\infty^{-1}$ , while  $\alpha_{sr}$  has been chosen equal to 0.25[20] or 1(DD-RSH-CAM[25]). However, this approach relies on global parameters and is not expected to perform accurately in systems composed of regions with significant dielectric mismatch.

To address the limitations of the DDH and RS-DDH functionals, we developed the screened-exchange range-separated hybrid (SE-RSH) functional, which provides a more general framework by incorporating local variations of the dielectric screening. The SE-RSH

mixing fraction is defined as:

$$\alpha^{\text{SE-RSH}}(\mathbf{r}, \mathbf{r}') = \frac{1}{\sqrt{\varepsilon(\mathbf{r})\varepsilon(\mathbf{r}')}} + \left(1 - \frac{1}{\sqrt{\varepsilon(\mathbf{r})\varepsilon(\mathbf{r}')}}\right) \text{erfc}(\mu(\mathbf{r})|\mathbf{r} - \mathbf{r}'|). \quad (3)$$

Here,  $\varepsilon(\mathbf{r})$  and  $\mu(\mathbf{r})$  represent a local dielectric function and local screening function, respectively;  $\varepsilon(\mathbf{r})$  is determined from DFT calculations in finite electric field, by evaluating the shifts of Wannier function centers in the presence of a static field to obtain the spatially dependent induced polarization.[47–49]. Fig.(1) illustrates the distinct dielectric screening profiles of a covalently bonded semiconductor (SiC) and a metal oxide (ZnO). The significant ionic character of metal-oxygen bonds in ZnO leads to strong variations in the local charge density near each ion, resulting in a highly position-dependent polarizability. By explicitly incorporating  $\varepsilon(\mathbf{r})$  rather than a single global  $\varepsilon_\infty$  parameter, the SE-RSH functional effectively captures the local screening fluctuations and their impact on the electronic structure of the material. This sensitivity to local screening is particularly valuable for systems with

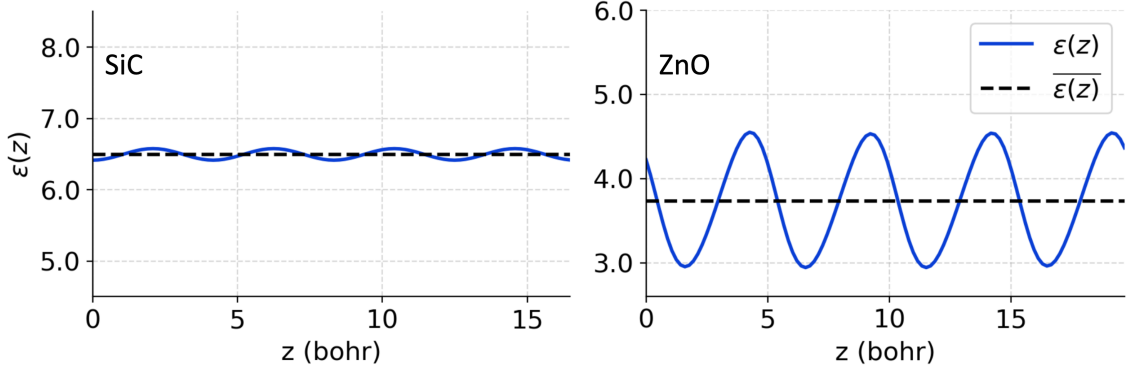


FIG. 1. Comparison of the local dielectric function ( $\varepsilon(z)$ ), average of the dielectric function  $\varepsilon(\mathbf{r})$  in the  $(x, y)$  plane) between SiC and ZnO.

ions in distinct oxidation states. For instance, when using a DFT+U [50] method to study  $\text{Co}_3\text{O}_4$ , the presence of different oxidation states requires two separate Hubbard U parameters [51]; however, as shown in Fig.(2), the SE-RSH functional naturally accounts for the differences in screening around each ion.

The local screening function  $\mu(\mathbf{r})$  generalizes the global  $\mu$  parameter used in RS-DDH. Previous work by Skone et al.[20] and Chen et al.[25] determined  $\mu$  by fitting a model dielectric function:

$$\varepsilon_{\text{model}}^{-1}(\mathbf{G}) = \varepsilon_\infty^{-1} + (1 - \varepsilon_\infty^{-1}) \left(1 - e^{-\frac{|\mathbf{G}|^2}{4\mu^2}}\right) \quad (4)$$

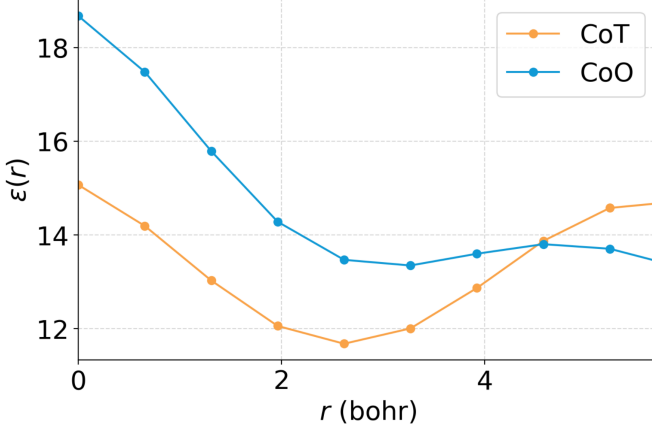


FIG. 2. Comparison of the local dielectric function  $\varepsilon(r)$ , computed as the spherical average of  $\varepsilon(\mathbf{r})$ , centered on two nonequivalent Co ions in  $\text{Co}_3\text{O}_4$ :  $\text{Co}^{2+}$  with tetrahedral oxygen coordination (CoT) and  $\text{Co}^{3+}$  with octahedral oxygen coordination (CoO).

to the long-range decay of the diagonal elements of the dielectric matrix  $\varepsilon^{-1}(\mathbf{G}, \mathbf{G}')$  computed using, for example, the linear response techniques proposed in Ref.[52] and implemented in the open-source **WEST** (Without Empty STates) code[53, 54]. This approach is formally equal to approximating the screened Coulomb interaction  $W(\mathbf{r}, \mathbf{r}')$  as:

$$W(\mathbf{r}, \mathbf{r}') = \int \varepsilon^{-1}(\mathbf{r}, \mathbf{r}'') v(\mathbf{r}'', \mathbf{r}') d\mathbf{r}'' \approx \frac{\varepsilon_\infty^{-1}}{|\mathbf{r} - \mathbf{r}'|} + (1 - \varepsilon_\infty^{-1}) \frac{\text{erfc}(\mu|\mathbf{r} - \mathbf{r}'|)}{|\mathbf{r} - \mathbf{r}'|}. \quad (5)$$

We extend this approximation by considering a generalized model  $W(\mathbf{r}, \mathbf{r}')$ , assuming that a local screening function  $\mu(\mathbf{r})$  is sufficient to capture the screening decay near a given point  $\{\mathbf{r}\}$ :

$$W(\mathbf{r}, \mathbf{r}') \approx \frac{\varepsilon^{-1}(\mathbf{r})}{|\mathbf{r} - \mathbf{r}'|} + (1 - \varepsilon^{-1}(\mathbf{r})) \frac{\text{erfc}(\mu(\mathbf{r})|\mathbf{r} - \mathbf{r}'|)}{|\mathbf{r} - \mathbf{r}'|}. \quad (6)$$

This generalization leads to a spatially resolved model for the dielectric function, as the Fourier transform of  $W(\mathbf{r}, \mathbf{r}')$  in Eq.(6) with respect to  $\mathbf{r}'$  is:

$$W(\mathbf{r}, \mathbf{G}') = \left[ \varepsilon^{-1}(\mathbf{r}) + (1 - \varepsilon^{-1}(\mathbf{r})) \left( 1 - e^{-\frac{|\mathbf{G}'|^2}{4\mu^2(\mathbf{r})}} \right) \right] e^{-i\mathbf{G}' \cdot \mathbf{r}} \frac{4\pi}{|\mathbf{G}'|^2} \quad (7)$$

$$= \varepsilon_{\text{model}}^{-1}(\mathbf{r}, \mathbf{G}') v(\mathbf{G}'), \quad (8)$$

where  $v(\mathbf{G}') = 4\pi/|\mathbf{G}'|^2$ . We can then determine  $\mu(\mathbf{r})$  through a fitting procedure:

$$\mu_{\text{fit}}(\mathbf{r}) = \underset{\mu(\mathbf{r})}{\text{argmin}} \sum_{\mathbf{G}'} \left| \varepsilon_{\text{model}}^{-1}(\mathbf{r}, \mathbf{G}') - \varepsilon^{-1}(\mathbf{r}, \mathbf{G}') \right|^2. \quad (9)$$

However, the direct implementation of this protocol would be computationally demanding, requiring the calculations of the dielectric function at each  $\{\mathbf{r}\}$  point in real space. To address this challenge, we approximate  $\mu_{\text{fit}}(\mathbf{r})$  using quantities that can be easily computed from first principles. Through an analysis of the value of  $\mu_{\text{fit}}(\mathbf{r})$  across diverse materials at randomly selected  $\{\mathbf{r}\}$  points, we found that the following approximation is accurate:

$$\mu_{\text{fit}}(\mathbf{r}) \approx \max(\mu_{\text{WS}}(\mathbf{r}), \mu_{\text{TF}}(\mathbf{r})) \quad (10)$$

as shown in Fig.(3), where  $\mu_{\text{WS}}(\mathbf{r}) = \frac{1}{r_s(\mathbf{r})} = \left(\frac{4\pi n_v(\mathbf{r})}{3}\right)^{1/3}$ ,  $\mu_{\text{TF}}(\mathbf{r}) = \frac{1}{2}k_{\text{TF}} = \left(\frac{3n_v(\mathbf{r})}{\pi}\right)^{1/6}$ ,  $n_v$  is the valence electron density,  $r_s$  is the Wigner-Seitz radius, and  $k_{\text{TF}}$  is the Thomas–Fermi screening wavevector. We note that  $\mu_{\text{WS}}$  can be interpreted as providing a measure of how

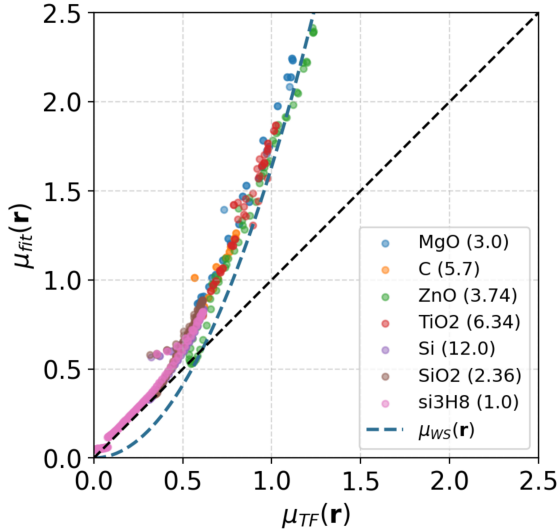


FIG. 3. Comparison of  $\mu_{\text{fit}}(\mathbf{r})$  (see Eq.(9)) with  $\mu_{\text{WS}}(\mathbf{r})$  and  $\mu_{\text{TF}}(\mathbf{r})$  (see text) at randomly selected points in real space  $\{\mathbf{r}\}$ , for several materials with different band gaps and dielectric constants (values in parentheses).

tightly electrons are packed in the material, while  $\mu_{\text{TF}}$  describes the collective response of the electron gas to external perturbations. By taking the maximum of the two values,  $\mu_{\text{fit}}$  ensures that the dominant screening mechanism in the system (whether local or collective) is adequately described.

## B. Computational Details

The SE-RSH hybrid functional has been implemented in a modified version of the `Qbox`[55] code, which employs a plane-wave basis set and norm-conserving pseudopotentials. We performed calculations for 13 metal oxides at the experimental geometry, using supercells containing between 128 and 256 atoms (see Supplementary Table ?? for details), and the  $\Gamma$  point to sample the supercell Brillouin zone. We used optimized norm-conserving Vanderbilt pseudopotentials[56]; semicore states were included for alkaline earth metals and (post-)transition metals. The energy cutoff for the plane-wave basis set was set at 90 Ry. The local dielectric function was determined self-consistently using the SE-RSH functional: at the first iteration, we performed a DFT calculation at the PBE level ( $\alpha(\mathbf{r}, \mathbf{r}') = 0$ ); then we set  $\varepsilon(\mathbf{r})$  in Eq.(3) to be the local dielectric function from the previous iteration until  $\varepsilon(\mathbf{r})$  and the total energy were converged.

The `WEST`[53, 54] code was used to compute the dielectric matrix using  $6 \times N_{\text{elec}}$  eigenpotentials for each system considered here, where  $N_{\text{elec}}$  is the number of electrons. The local screening function  $\mu(\mathbf{r})$  used in SE-RSH was computed according to Eq.(10).

## III. ELECTRONIC STRUCTURE OF OXIDES USING THE SE-RSH FUNCTIONAL

### A. Screening parameter and macroscopic dielectric constant

We computed the global screening parameters  $\mu$  for 13 oxides obtained by a least-squares fit to the dielectric functions and we compared our results with those of Ref.[25] (see Fig.(4) and Supplementary Table ??). Our calculated values differ from those of Ref.[25], most likely due to methodological differences in computing the dielectric matrix or the irreducible polarizability  $\chi^0$ . Chen et al. obtained the noninteracting Green's function  $G$  through a perturbative expansion over the Kohn-Sham eigenstates, requiring a convergence of the results with respect to the number of unoccupied states; instead we employed the projective dielectric eigenpotential (PDEP) approach[52] implemented in the `WEST` code[53, 54]. The PDEP method computes the dielectric matrix without the explicit evaluation of empty electronic states, with the accuracy controlled solely by the size of the PDEP basis set ( $N_{\text{PDEP}}$ ). We verified the convergence of  $\mu$  with respect to  $N_{\text{PDEP}}$ , as demonstrated in

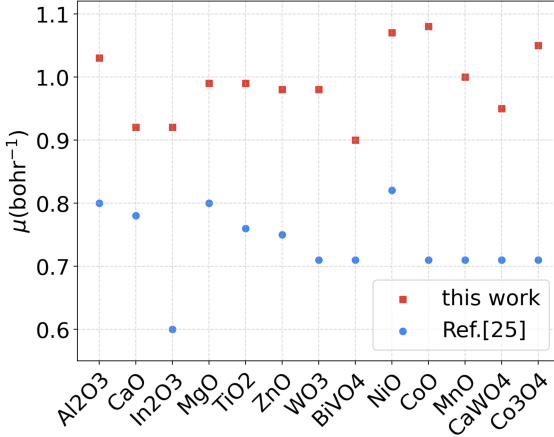


FIG. 4. Comparison of global screening parameters  $\mu$  from least-squares fits of the dielectric functions with those reported in Ref. [25] (see Supplementary Table ?? for details).

Fig.(5). As we show below, the value of the screening parameter  $\mu$  strongly influences the electronic structure predictions of the DD-RSH-CAM functional, making the methodological differences in computing the dielectric matrix particularly significant for accurate band gap predictions.

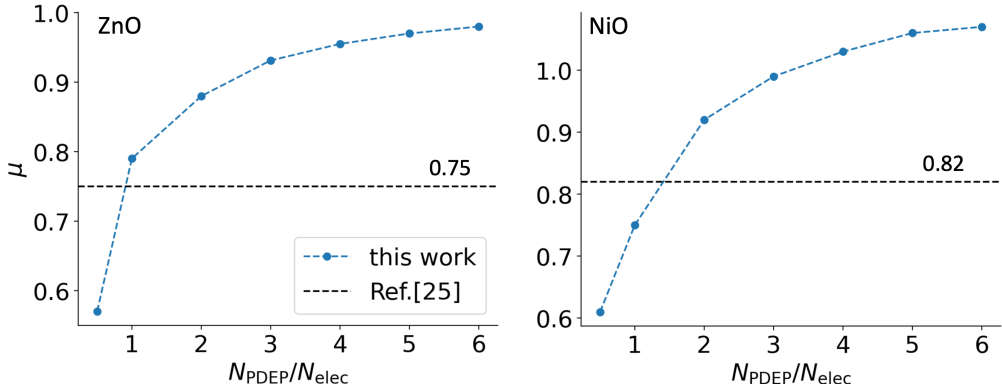


FIG. 5. The global screening parameters  $\mu$  of ZnO and NiO, computed by fitting the dielectric functions, as a function of the ratio of the projective dielectric eigenpotential (PDEP)[52] basis set size to the number of electrons. For comparison, horizontal dashed lines indicate the  $\mu$  values for both systems as reported in Ref.[25] and used by DD-RSH-CAM.

Fig.(6) also presents macroscopic dielectric constants ( $\varepsilon_\infty$ ) computed using both the finite field (FF) method at the PBE level and self-consistently at the hybrid functional level. For DD-RSH-CAM calculations, we fixed  $\mu$  to the values specified in Supplementary Table ??.

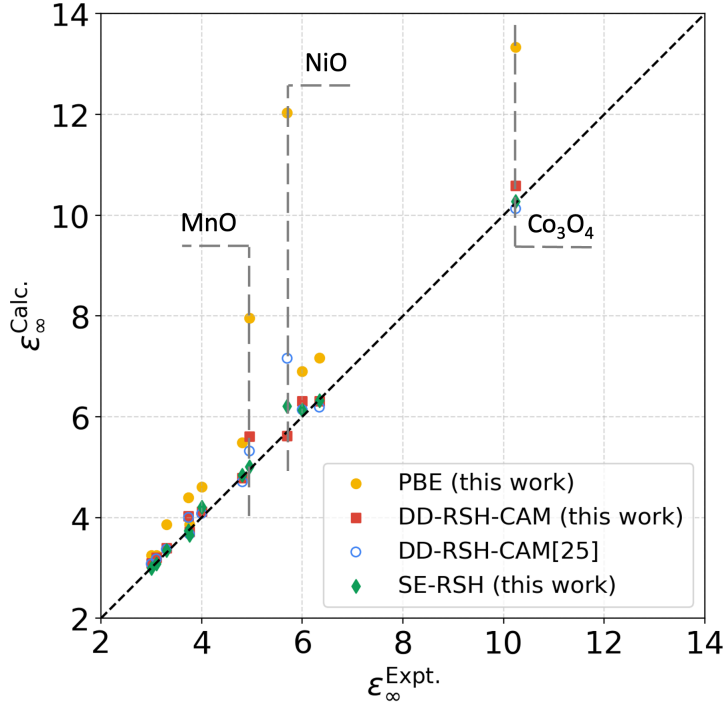


FIG. 6. Comparison of experimental macroscopic dielectric constants  $\varepsilon_{\infty}^{\text{Expt.}}$  with calculated values  $\varepsilon_{\infty}^{\text{Calc.}}$  using the finite-field method at the PBE level and self-consistently at the level of dielectric-dependent hybrid functionals (see Supplementary Table ?? for details). See text for the definition of the DD-RSH-CAM and SE-RSH functionals.

The finite field approach based on the PBE functional (FF@PBE) systematically overestimates  $\varepsilon_\infty$  compared to the experimental values, with particularly pronounced deviations for strongly correlated Mott insulators such as NiO and MnO. In contrast, FF@hybrid calculations significantly improve the accuracy of our results, with SE-RSH achieving a mean absolute percentage error (MAPE) of just 2.34% (details are shown in Supplementary Table ??). Additionally, we note that the self-consistent determination of dielectric constants using FF@hybrid typically converges within a few iterations, as shown in Fig.(7).

## B. Band gap

In Fig.(8), we compare the band gaps obtained for oxides using the SE-RSH hybrid functional and other dielectric-dependent hybrid functionals, including the DD-RSH-CAM which utilizes  $\frac{1}{\varepsilon_\infty}$  as the fraction of Fock exchange in the long-range part and a constant screening parameter  $\mu$ . To evaluate the impact of the choice of  $\mu$  on the performance of

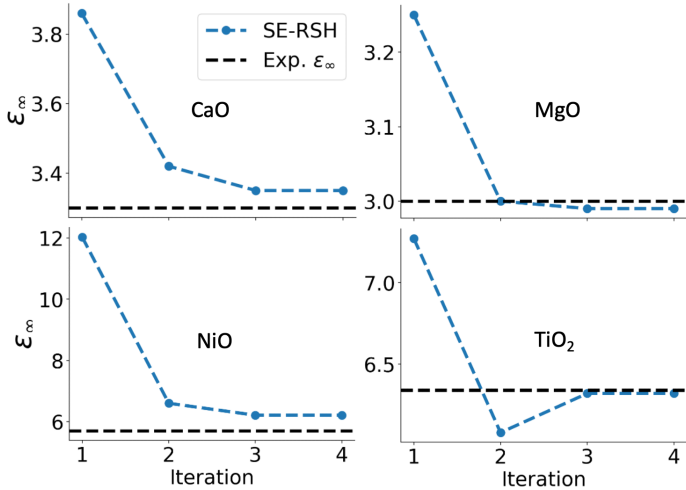


FIG. 7. Macroscopic dielectric constants of CaO, MgO, NiO and TiO<sub>2</sub>, computed using the finite field method at the level of SE-RSH, as a function of the number of iteration of the self-consistent procedure. The horizontal dash lines denote experimental values.

DD-RSH-CAM, we present results using both our own computed values (see computational details) and those from Ref.[25]. Because our calculations do not include electron–phonon coupling, we subtract the value of the zero-phonon renormalization (ZPR) from computed band gaps, where available, for a comparison with experimental data. The ZPR values are also shown in Supplementary Table ??.

The SE-RSH functional yields accurate band gaps for most of the systems studied, with a mean error (ME) of 0.09 eV and a mean absolute error (MAE) of 0.26 eV (see Supplementary Table ?? for details). For some oxides, such as NiO and Co<sub>3</sub>O<sub>4</sub>, whose band gaps are typically overestimated by DD-RSH-CAM, the SE-RSH tends to yield predictions closer to experiments. This improved accuracy arises primarily from the SE-RSH’s ability to capture variations in the local dielectric screening of metal oxides, even though both functionals are formally equivalent when  $\epsilon(\mathbf{r})$  and  $\mu(\mathbf{r})$  are constant. We note that for certain oxides, such as Al<sub>2</sub>O<sub>3</sub>, MgO, CaWO<sub>4</sub> and Co<sub>3</sub>O<sub>4</sub>, SE-RSH slightly overestimates the band gap; however, no ZPR values for these oxides are available and hence they were not subtracted. Additionally, for WO<sub>3</sub> and Co<sub>3</sub>O<sub>4</sub>, the discrepancy between SE-RSH and experimental values exceeds 10%. This large difference may be partly attributed to experimental data collected from thin films[57] or under conditions with high surface sensitivity[58], which might lead to differences from bulk values.

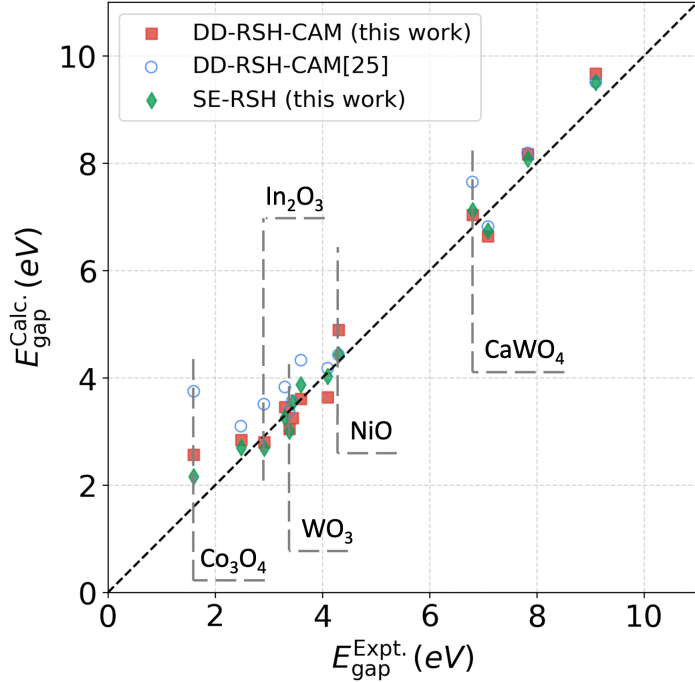


FIG. 8. Fundamental band gaps  $E_{\text{gap}}^{\text{Calc.}}$  (eV) computed for 13 metal oxides, compared with experimental values  $E_{\text{gap}}^{\text{Expt.}}$  (eV) (see Supplementary Table ?? for details).

It is worth noting that some of the DD-RSH-CAM results reported here differ from those of Ref.[25]. Specifically, our calculated DD-RSH-CAM band gaps are smaller for a few compounds (including  $\text{In}_2\text{O}_3$ ,  $\text{TiO}_2$ ,  $\text{ZnO}$ ), a difference due to our computed values for  $\mu$  (see Section III A). The only exception is  $\text{NiO}$ , for which our DD-RSH-CAM calculations predict a larger gap, primarily due to differences in the calculated dielectric constant. To better understand the effect of  $\mu$ , we performed additional calculations using experimental dielectric constants. For  $\text{NiO}$ , we find a significantly overestimated band gap of 5.7 eV when using  $\mu = 0.82$  from Ref.[25], suggesting this  $\mu$  value may be inappropriate. While our computed  $\mu$  values overall improve the accuracy of DD-RSH-CAM, this functional still yields overestimated gaps for  $\text{NiO}$  and  $\text{Co}_3\text{O}_4$ , indicating that an accurate treatment of the spatially varying dielectric screening is crucial for these systems.

### C. Magnetic moment of antiferromagnetic TMO

Finally, we assess the performance of SE-RSH in predicting magnetic moments of anti-ferromagnetic transition metal oxides. Table I presents calculated magnetic moments using

different functionals alongside experimental values. The PBE functional underestimates magnetic moments, consistent with its known tendency to over delocalize electrons. Hybrid functionals, including SE-RSH, produce larger magnetic moments in closer agreement with experimental data. Notably, the predicted magnetic moments show relatively low sensitivity to the specific hybrid functional employed, suggesting that the specific treatment of exact exchange plays a less critical role in determining magnetic properties than it does for band gaps and dielectric constants, at least for the materials studied here.

TABLE I. Magnetic moments (in  $\mu\text{B}/\text{atom}$ ) calculated by several functionals as well as from available experimental values.

	PBE	DD-RSH-CAM	SE-RSH	Expt.
NiO	1.19	1.67	1.66	1.64[59], 1.90[60]
MnO	4.08	4.46	4.52	4.58[61]
CoO	2.24	2.76	2.71	2.46[62]

#### IV. CONCLUSIONS

In summary, we have presented a comprehensive assessment of the SE-RSH functional for metal oxides by computing band gaps, dielectric constants and magnetic moments, and comparing our results with those of other range-separated dielectric-dependent hybrid functionals and with experiments. The key innovation of the SE-RSH functional lies in its spatially resolved treatment of the dielectric screening, incorporating both local dielectric and screening functions in determining the exact-exchange mixing fraction. This approach enables an accurate treatment of the local variations in the dielectric screening characteristic of metal oxides. We find that SE-RSH can predict fundamental band gaps, dielectric constants, and magnetic moments in close agreement with experiments. Our results underscore the importance of self-consistently computing the macroscopic dielectric constant at the hybrid functional level, as this corrects the significant overestimation observed at the PBE level of theory. Furthermore, our analysis reveals that different implementations can yield substantially different screening parameters  $\mu$ , helping to explain previously reported band gap overestimates by the DD-RSH-CAM functional for certain systems. Work is in progress

to extending the application of the SE-RSH functional to investigate oxide-oxide and oxide-water interfaces[63], where the accurate treatment of spatially varying dielectric screening is particularly crucial for understanding electrochemical and photocatalytic processes.

## ACKNOWLEDGMENTS

The authors thank Yu Jin for valuable discussions. This work was supported by DOE/BES through the Computational Materials Science Center Midwest Integrated Center for Computational Materials (MICCoM). The computational resources were provided by the University of Chicago's Research Computing Center and the National Energy Research Scientific Computing Center (NERSC).

---

- [1] M. S. S. Danish, A. Bhattacharya, D. Stepanova, A. Mikhaylov, M. L. Grilli, M. Khosravy, and T. Senju, A systematic review of metal oxide applications for energy and environmental sustainability, *Metals* **10**, 1604 (2020).
- [2] P. Pazhamalai, V. Krishnan, M. S. Mohamed Saleem, S.-J. Kim, and H.-W. Seo, Investigating composite electrode materials of metal oxides for advanced energy storage applications, *Nano Convergence* **11**, 30 (2024).
- [3] G. Wang, Y. Yang, D. Han, and Y. Li, Oxygen defective metal oxides for energy conversion and storage, *Nano Today* **13**, 23 (2017).
- [4] T. Naseem and T. Durrani, The role of some important metal oxide nanoparticles for wastewater and antibacterial applications: A review, *Environmental Chemistry and Ecotoxicology* **3**, 59 (2021).
- [5] G. F. Fine, L. M. Cavanagh, A. Afonja, and R. Binions, Metal oxide semi-conductor gas sensors in environmental monitoring, *sensors* **10**, 5469 (2010).
- [6] A. Kudo and Y. Miseki, Heterogeneous photocatalyst materials for water splitting, *Chemical Society Reviews* **38**, 253 (2009).
- [7] F. E. Osterloh, Inorganic materials as catalysts for photochemical splitting of water, *Chemistry of Materials* **20**, 35 (2008).

- [8] R. Jose, V. Thavasi, and S. Ramakrishna, Metal oxides for dye-sensitized solar cells, *Journal of the American Ceramic Society* **92**, 289 (2009).
- [9] S. Royer and D. Duprez, Catalytic oxidation of carbon monoxide over transition metal oxides, *ChemCatChem* **3**, 24 (2011).
- [10] L. Hedin, New method for calculating the one-particle green's function with application to the electron-gas problem, *Physical Review* **139**, A796 (1965).
- [11] R. M. Martin, L. Reining, and D. M. Ceperley, *Interacting electrons* (Cambridge University Press, 2016).
- [12] J. Tomasi, B. Mennucci, and R. Cammi, Quantum mechanical continuum solvation models, *Chemical reviews* **105**, 2999 (2005).
- [13] F. Lipparini and B. Mennucci, Perspective: Polarizable continuum models for quantum-mechanical descriptions, *The Journal of chemical physics* **144** (2016).
- [14] O. Andreussi, I. Dabo, and N. Marzari, Revised self-consistent continuum solvation in electronic-structure calculations, *The Journal of chemical physics* **136** (2012).
- [15] M. Shishkin and G. Kresse, Self-consistent gw calculations for semiconductors and insulators, *Physical Review B—Condensed Matter and Materials Physics* **75**, 235102 (2007).
- [16] C. Adamo and V. Barone, Toward reliable density functional methods without adjustable parameters: The pbe0 model, *The Journal of chemical physics* **110**, 6158 (1999).
- [17] J. Heyd, G. E. Scuseria, and M. Ernzerhof, Hybrid functionals based on a screened coulomb potential, *The Journal of chemical physics* **118**, 8207 (2003).
- [18] J. Heyd, G. E. Scuseria, and M. Ernzerhof, Erratum: “hybrid functionals based on a screened coulomb potential” [j. chem. phys. 118, 8207 (2003)], *The Journal of Chemical Physics* **124**, 219906 (2006), [https://pubs.aip.org/aip/jcp/article-pdf/doi/10.1063/1.2204597/15387022/219906\\_1\\_online.pdf](https://pubs.aip.org/aip/jcp/article-pdf/doi/10.1063/1.2204597/15387022/219906_1_online.pdf).
- [19] A. V. Krukau, O. A. Vydrov, A. F. Izmaylov, and G. E. Scuseria, Influence of the exchange screening parameter on the performance of screened hybrid functionals, *The Journal of chemical physics* **125** (2006).
- [20] J. H. Skone, M. Govoni, and G. Galli, Nonempirical range-separated hybrid functionals for solids and molecules, *Physical Review B* **93**, 235106 (2016).
- [21] J. H. Skone, M. Govoni, and G. Galli, Self-consistent hybrid functional for condensed systems, *Physical Review B* **89**, 195112 (2014).

- [22] M. A. Marques, J. Vidal, M. J. Oliveira, L. Reining, and S. Botti, Density-based mixing parameter for hybrid functionals, *Physical Review B—Condensed Matter and Materials Physics* **83**, 035119 (2011).
- [23] Z.-H. Cui, Y.-C. Wang, M.-Y. Zhang, X. Xu, and H. Jiang, Doubly screened hybrid functional: an accurate first-principles approach for both narrow-and wide-gap semiconductors, *The Journal of Physical Chemistry Letters* **9**, 2338 (2018).
- [24] N. P. Brawand, M. Govoni, M. Vörös, and G. Galli, Performance and self-consistency of the generalized dielectric dependent hybrid functional, *Journal of chemical theory and computation* **13**, 3318 (2017).
- [25] W. Chen, G. Miceli, G.-M. Rignanese, and A. Pasquarello, Nonempirical dielectric-dependent hybrid functional with range separation for semiconductors and insulators, *Physical Review Materials* **2**, 073803 (2018).
- [26] M. Gerosa, C. E. Bottani, L. Caramella, G. Onida, C. Di Valentin, and G. Pacchioni, Defect calculations in semiconductors through a dielectric-dependent hybrid dft functional: The case of oxygen vacancies in metal oxides, *The Journal of chemical physics* **143** (2015).
- [27] A. P. Gaiduk, T. A. Pham, M. Govoni, F. Paesani, and G. Galli, Electron affinity of liquid water, *Nature communications* **9**, 247 (2018).
- [28] T. A. Pham, M. Govoni, R. Seidel, S. E. Bradforth, E. Schwegler, and G. Galli, Electronic structure of aqueous solutions: Bridging the gap between theory and experiments, *Science advances* **3**, e1603210 (2017).
- [29] P. Liu, C. Franchini, M. Marsman, and G. Kresse, Assessing model-dielectric-dependent hybrid functionals on the antiferromagnetic transition-metal monoxides mno, feo, coo, and nio, *Journal of Physics: Condensed Matter* **32**, 015502 (2019).
- [30] T. Das, G. Di Liberto, S. Tosoni, and G. Pacchioni, Band gap of 3d metal oxides and quasi-2d materials from hybrid density functional theory: are dielectric-dependent functionals superior?, *Journal of chemical theory and computation* **15**, 6294 (2019).
- [31] G. Borghi, A. Ferretti, N. L. Nguyen, I. Dabo, and N. Marzari, Koopmans-compliant functionals and their performance against reference molecular data, *Physical Review B* **90**, 075135 (2014).
- [32] N. Colonna, N. L. Nguyen, A. Ferretti, and N. Marzari, Koopmans-compliant functionals and potentials and their application to the gw100 test set, *Journal of chemical theory and*

computation **15**, 1905 (2019).

- [33] N. L. Nguyen, N. Colonna, A. Ferretti, and N. Marzari, Koopmans-compliant spectral functionals for extended systems, *Physical Review X* **8**, 021051 (2018).
- [34] N. Colonna, R. De Gennaro, E. Linscott, and N. Marzari, Koopmans spectral functionals in periodic boundary conditions, *Journal of Chemical Theory and Computation* **18**, 5435 (2022).
- [35] J. Ma and L.-W. Wang, Using wannier functions to improve solid band gap predictions in density functional theory, *Scientific reports* **6**, 24924 (2016).
- [36] M. Weng, S. Li, J. Ma, J. Zheng, F. Pan, and L.-W. Wang, Wannier koopman method calculations of the band gaps of alkali halides, *Applied Physics Letters* **111** (2017).
- [37] M. Weng, S. Li, J. Zheng, F. Pan, and L.-W. Wang, Wannier koopmans method calculations of 2d material band gaps, *The Journal of Physical Chemistry Letters* **9**, 281 (2018).
- [38] M. Weng, F. Pan, and L.-W. Wang, Wannier–koopmans method calculations for transition metal oxide band gaps, *npj Computational Materials* **6**, 33 (2020).
- [39] J. Zhan, M. Govoni, and G. Galli, Nonempirical range-separated hybrid functional with spatially dependent screened exchange, *Journal of Chemical Theory and Computation* **19**, 5851 (2023).
- [40] T. Leininger, H. Stoll, H.-J. Werner, and A. Savin, Combining long-range configuration interaction with short-range density functionals, *Chemical physics letters* **275**, 151 (1997).
- [41] O. A. Vydrov and G. E. Scuseria, Assessment of a long-range corrected hybrid functional, *The Journal of chemical physics* **125** (2006).
- [42] O. A. Vydrov, J. Heyd, A. V. Krukau, and G. E. Scuseria, Importance of short-range versus long-range hartree-fock exchange for the performance of hybrid density functionals, *The Journal of chemical physics* **125** (2006).
- [43] T. Yanai, D. P. Tew, and N. C. Handy, A new hybrid exchange–correlation functional using the coulomb-attenuating method (cam-b3lyp), *Chemical physics letters* **393**, 51 (2004).
- [44] J.-D. Chai and M. Head-Gordon, Long-range corrected hybrid density functionals with damped atom–atom dispersion corrections, *Physical Chemistry Chemical Physics* **10**, 6615 (2008).
- [45] T. Stein, L. Kronik, and R. Baer, Reliable prediction of charge transfer excitations in molecular complexes using time-dependent density functional theory, *Journal of the American Chemical Society* **131**, 2818 (2009).

- [46] R. Baer, E. Livshits, and U. Salzner, Tuned range-separated hybrids in density functional theory, *Annual review of physical chemistry* **61**, 85 (2010).
- [47] H. Zheng, M. Govoni, and G. Galli, Dielectric-dependent hybrid functionals for heterogeneous materials, *Physical Review Materials* **3**, 073803 (2019).
- [48] M. Stengel and N. A. Spaldin, Accurate polarization within a unified wannier function formalism, *Physical Review B—Condensed Matter and Materials Physics* **73**, 075121 (2006).
- [49] I. Souza, J. Íñiguez, and D. Vanderbilt, First-principles approach to insulators in finite electric fields, *Physical review letters* **89**, 117602 (2002).
- [50] V. I. Anisimov, J. Zaanen, and O. K. Andersen, Band theory and mott insulators: Hubbard  $u$  instead of stoner  $i$ , *Physical Review B* **44**, 943 (1991).
- [51] J. Chen, X. Wu, and A. Selloni, Electronic structure and bonding properties of cobalt oxide in the spinel structure, *Physical Review B—Condensed Matter and Materials Physics* **83**, 245204 (2011).
- [52] H. F. Wilson, F. Gygi, and G. Galli, Efficient iterative method for calculations of dielectric matrices, *Physical Review B—Condensed Matter and Materials Physics* **78**, 113303 (2008).
- [53] M. Govoni and G. Galli, Large scale gw calculations, *Journal of chemical theory and computation* **11**, 2680 (2015).
- [54] V. W.-z. Yu and M. Govoni, Gpu acceleration of large-scale full-frequency gw calculations, *Journal of Chemical Theory and Computation* **18**, 4690 (2022).
- [55] F. Gygi, Architecture of qbox: A scalable first-principles molecular dynamics code, *IBM Journal of Research and Development* **52**, 137 (2008).
- [56] D. Hamann, Optimized norm-conserving vanderbilt pseudopotentials, *Physical Review B—Condensed Matter and Materials Physics* **88**, 085117 (2013).
- [57] V. Shinde, S. Mahadik, T. Gujar, and C. Lokhande, Supercapacitive cobalt oxide (co<sub>3</sub>o<sub>4</sub>) thin films by spray pyrolysis, *Applied Surface Science* **252**, 7487 (2006).
- [58] J. Meyer, M. Kröger, S. Hamwi, F. Gnam, T. Riedl, W. Kowalsky, and A. Kahn, Charge generation layers comprising transition metal-oxide/organic interfaces: Electronic structure and charge generation mechanism, *Applied Physics Letters* **96** (2010).
- [59] H. Aplerin, The magnetic form factor of nickel oxide, *J. Phys. Soc. Japan* **17** (1962).
- [60] W. Roth, Magnetic structures of mno, feo, coo, and nio, *Physical Review* **110**, 1333 (1958).

- [61] A. Cheetham and D. Hope, Magnetic ordering and exchange effects in the antiferromagnetic solid solutions  $\text{mn}_x \text{ni}_{1-x} \text{o}$ , *Physical Review B* **27**, 6964 (1983).
- [62] S. Csiszar, M. Haverkort, Z. Hu, A. Tanaka, H. Hsieh, H.-J. Lin, C. Chen, T. Hibma, and L. Tjeng, Controlling orbital moment and spin orientation in coo layers by strain, *Physical Review Letters* **95**, 187205 (2005).
- [63] M. Bousquet, J. Zhan, C. Luo, A. B. Martinson, F. Gygi, and G. Galli, in preparation.

# Supporting Information: Dielectric-Dependent Range-Separated Hybrid Functional Calculations for Metal Oxides

Jiawei Zhan,<sup>1</sup> Marco Govoni,<sup>1,2,3</sup> and Giulia Galli<sup>1,2,4,\*</sup>

<sup>1</sup>*Pritzker School of Molecular Engineering,*

*University of Chicago, Chicago, Illinois 60637, United States*

<sup>2</sup>*Materials Science Division and Center for Molecular Engineering,  
Argonne National Laboratory, Lemont, Illinois 60439, United States*

<sup>3</sup>*Department of Physics, Computer Science, and Mathematics,  
University of Modena and Reggio Emilia, Modena, 41125, Italy*

<sup>4</sup>*Department of Chemistry, University of Chicago,  
Chicago, Illinois 60637, United States*

(Dated: February 19, 2025)

---

\* [gagalli@uchicago.edu](mailto:gagalli@uchicago.edu)

TABLE S1. The space group, lattice parameters, and the number of atoms in the supercell used for the calculations of 13 oxides.

	Space group	a(Å)	b(Å)	c(Å)	$\alpha$ (°)	$\beta$ (°)	$\gamma$ (°)	Reference	# of atoms
Al <sub>2</sub> O <sub>3</sub>	<i>R</i> 3̄ <i>c</i>	4.760	4.760	12.990	90	90	90	[1]	240 <sup>a</sup>
CaO	<i>Fm</i> 3̄ <i>m</i>	4.803	4.803	4.803	90	90	90	[2]	256 <sup>a</sup>
In <sub>2</sub> O <sub>3</sub>	<i>Ia</i> 3̄	10.117	10.117	10.117	90	90	90	[3]	160 <sup>a</sup>
MgO	<i>Fm</i> 3̄ <i>m</i>	4.207	4.207	4.207	90	90	90	[2]	256 <sup>a</sup>
TiO <sub>2</sub>	<i>P</i> 4 <sub>2</sub> / <i>mnm</i>	4.593	4.593	2.958	90	90	90	[4]	192 <sup>a</sup>
ZnO	<i>P</i> 6 <sub>3</sub> <i>mc</i>	3.250	3.250	5.203	90	90	90	[5]	128 <sup>a</sup>
WO <sub>3</sub>	<i>P</i> 2 <sub>1</sub> / <i>c</i>	7.301	7.539	7.690	90	90.89	90	[6]	256 <sup>a</sup>
BiVO <sub>4</sub>	<i>I</i> 2/ <i>b</i>	5.190	5.090	11.700	90	90	90.38	[7]	192 <sup>a</sup>
NiO	<i>Fm</i> 3̄ <i>m</i>	4.171	4.171	4.171	90	90	90	[8]	256 <sup>b</sup>
CoO	<i>Fm</i> 3̄ <i>m</i>	4.254	4.254	4.254	90	90	90	[9]	256 <sup>b</sup>
MnO	<i>Fm</i> 3̄ <i>m</i>	4.445	4.445	4.445	90	90	90	[10]	256 <sup>b</sup>
CaWO <sub>4</sub>	<i>I</i> 4 <sub>1</sub> / <i>a</i>	5.249	5.249	11.393	90	90	90	[11]	144 <sup>a</sup>
Co <sub>3</sub> O <sub>4</sub>	<i>F</i> d3̄ <i>m</i>	8.084	8.084	8.084	90	90	90	[12]	224 <sup>a</sup>

<sup>a</sup> Supercell sizes were chosen to ensure convergence of the computed fundamental band gap values (see Fig. S1).

<sup>b</sup> We determined the appropriate size of the supercell by comparing the computed fundamental band gaps with those from primitive cell calculations using an 8×8×8 k-point mesh with a global dielectric-dependent hybrid functional. We chose  $\alpha = 1/\varepsilon_\infty$ , where  $\varepsilon_\infty$  is the experimental macroscopic dielectric constant, for this comparison. Results with 256-atom supercells yield band gaps of 3.47 eV, 3.20 eV, and 3.16 eV for NiO, CoO, and MnO, respectively, compared to 3.51 eV, 3.17 eV, and 3.09 eV obtained from the primitive cell calculations performed using **Quantum Espresso**.

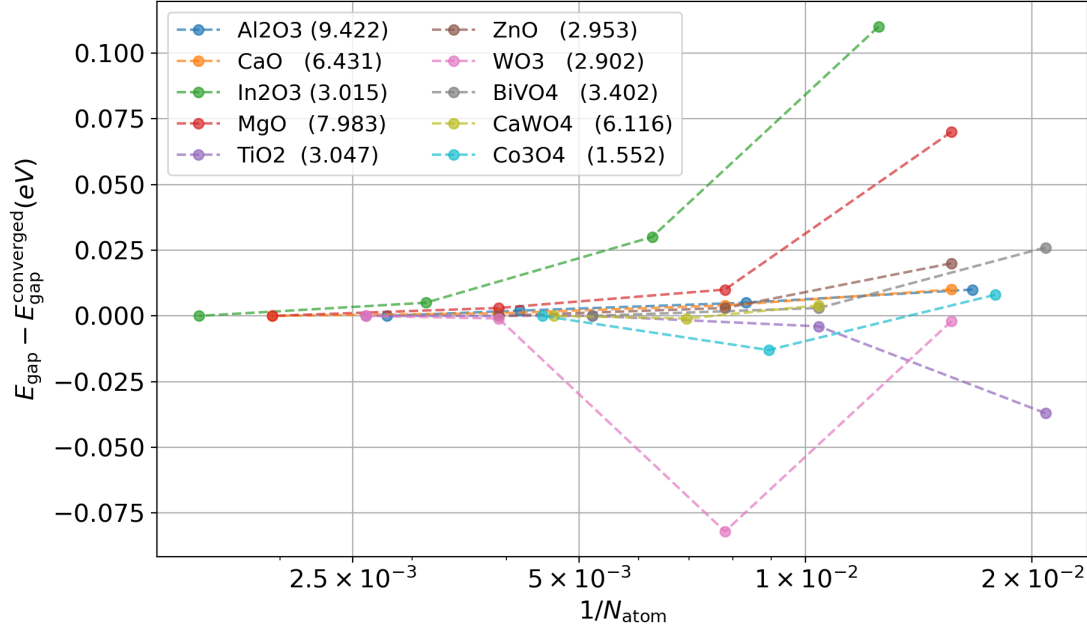


FIG. S1. Convergence of band gaps with increasing number of atoms ( $N_{\text{atom}}$ ) in the supercell, computed using the global dielectric-dependent hybrid functional ( $\alpha = 1/\varepsilon_{\infty}$ , where  $\varepsilon_{\infty}$  is the experimental macroscopic dielectric constant). Values in parentheses in the inset indicate the converged  $E_{\text{gap}}$  in eV.

TABLE S2. The global screening parameters  $\mu$  obtained in this work via least-squares fit to the dielectric functions compared with the values reported in Ref.[13] (columns 2 and 3). The macroscopic dielectric constants  $\varepsilon_\infty$  calculated using the finite-field method at the PBE level and self-consistently at the level of dielectric-dependent hybrid functionals are given in columns 4-7 and the experimental results in column 8. The mean error (ME), mean absolute error (MAE), and mean absolute percentage error (MAPE) relative to experimental dielectric constants are also reported.

	$\mu(\text{bohr}^{-1})$			$\varepsilon_\infty$			
	DD-RSH-CAM	DD-RSH-CAM[13]	PBE	DD-RSH-CAM	DD-RSH-CAM[13]	SE-RSH	Expt.
Al <sub>2</sub> O <sub>3</sub>	1.03	0.80	3.25	3.21	3.18	3.08	3.10
CaO	0.92	0.78	3.86	3.39	3.37	3.35	3.30
In <sub>2</sub> O <sub>3</sub>	0.92	0.60	4.61	4.12	4.08	4.21	4.00
MgO	0.99	0.80	3.25	3.09	3.08	2.99	3.00
TiO <sub>2</sub>	0.99	0.76	7.17	6.31	6.19	6.32	6.34
ZnO	0.98	0.75	4.40	4.03	4.00	3.74	3.74
WO <sub>3</sub>	0.98	0.71 <sup>a</sup>	5.49	4.79	4.71 <sup>b</sup>	4.84	4.81
BiVO <sub>4</sub>	0.90	0.71 <sup>a</sup>	6.90	6.31	6.14 <sup>b</sup>	6.13	6.00
NiO	1.07	0.82	12.03	5.62	7.16	6.21	5.70
CoO	1.08	0.71 <sup>a</sup>	—	5.63	5.29 <sup>b</sup>	4.97	5.30
MnO	1.00	0.71 <sup>a</sup>	7.96	5.61	5.32 <sup>b</sup>	5.01	4.95
CaWO <sub>4</sub>	0.95	0.71 <sup>a</sup>	3.86	3.72	3.67 <sup>b</sup>	3.65	3.76
Co <sub>3</sub> O <sub>4</sub>	1.05	0.71 <sup>a</sup>	13.34	10.59	10.13 <sup>b</sup>	10.27	10.24
ME			1.43	0.17	0.16	0.04	
MAE			1.43	0.19	0.23	0.12	
MAPE(%)			25.84	3.96	4.60	2.34	

<sup>a</sup>  $\mu$  is set to 0.71, in accordance with the recommendation in Ref.[13].

<sup>b</sup>  $\varepsilon_\infty$  is determined self-consistently using the finite-field method @ DD-RSH-CAM with  $\mu = 0.71$

TABLE S3. Fundamental band gaps  $E_g$ (eV) computed for 13 metal oxides; we subtracted from each theoretical value the zero-phonon renormalization (ZPR)  $E_{\text{ZPR}}$  (column 7) when available. Most experimental values are obtained from the optical gap extrapolated to 0 K, with the exciton binding energy added, when available. The ME, MAE, and MAPE values relative to  $E_{\text{Expt.}}$  are also reported.

	PBE	DD-RSH-CAM	DD-RSH-CAM[13]	SE-RSH	Expt.	$E_{\text{ZPR}}$
Al <sub>2</sub> O <sub>3</sub>	6.25	9.67	9.51	9.51	9.10 <sup>b</sup>	
CaO	3.26	6.64	6.82	6.74	7.09 <sup>c</sup>	0.35[14]
In <sub>2</sub> O <sub>3</sub>	1.21	2.80	3.51	2.69	2.91 <sup>d</sup>	
MgO	4.80	8.17	8.19	8.08	7.83 <sup>e</sup>	
TiO <sub>2</sub>	1.61	3.46	3.83	3.26	3.30 <sup>f</sup>	0.35[14]
ZnO	0.69	3.25	3.57	3.54	3.44 <sup>g</sup>	0.17[14]
WO <sub>3</sub>	1.51	3.05	3.38 <sup>a</sup>	3.01	3.38 <sup>h</sup>	0.4[15]
BiVO <sub>4</sub>	1.83(1.16 <sup>p</sup> )	3.52(2.85 <sup>p</sup> )	3.77 <sup>a</sup> (3.10 <sup>p</sup> )	3.37(2.70 <sup>p</sup> )	2.48 <sup>i</sup>	0.38[16]
NiO	0.72	4.90	4.43	4.44	4.30 <sup>j</sup>	0.25[17]
CoO	metal	3.61	4.33 <sup>a</sup>	3.88	3.60 <sup>k</sup>	0.28[17]
MnO	0.59	3.64	4.18 <sup>a</sup>	4.03	4.1 <sup>l</sup>	0.3[17]
CaWO <sub>4</sub>	4.13	7.04	7.65 <sup>a</sup>	7.12	6.8 <sup>m</sup>	
Co <sub>3</sub> O <sub>4</sub>	0.31	2.57	3.75 <sup>a</sup>	2.16	1.6 <sup>n</sup>	
ME	-2.51	0.13	0.49	0.09		
MAE	2.51	0.37	0.53	0.26		
MAPE(%)	59.2	11.2	19.3	7.4		

<sup>a</sup>Band gaps computed with DD-RSH-CAM using  $\varepsilon_{\infty}$  and  $\mu$  from Table S2; <sup>b</sup>Ref.[18], optical band gap extrapolated to 0 K; <sup>c</sup>Ref.[19] at 85 K; <sup>d</sup>Optical band gap extrapolated to 0 K[20] plus exciton binding energy[21]; <sup>e</sup>Ref.[19] at 85 K; <sup>f</sup>Ref.[22]; <sup>g</sup>Ref.[23] at 6 K; <sup>h</sup>Ref.[24]; <sup>i</sup>Ref.[25]; <sup>j</sup>Ref.[26] at 473 K; <sup>k</sup>Ref.[27] via conductivity measurement, referring to 0K; <sup>l</sup>Ref.[28]; <sup>m</sup>Exciton reflectance peak at 295 K [29] plus exciton binding energy[30]; <sup>n</sup>Ref.[31], optical band gap at 300 K. <sup>p</sup>Spin-orbit coupling and nuclear quantum effects are also considered[16].

---

- [1] S. Kondo, K. Tateishi, and N. Ishizawa, Structural evolution of corundum at high temperatures, *Japanese journal of applied physics* **47**, 616 (2008).
- [2] D. K. Smith and H. Leider, Low-temperature thermal expansion of lih, mgo and cao, *Journal of Applied Crystallography* **1**, 246 (1968).
- [3] M. Marezio, Refinement of the crystal structure of in2o3 at two wavelengths, *Acta Crystallographica* **20**, 723 (1966).
- [4] J. K. Burdett, T. Hughbanks, G. J. Miller, J. W. Richardson Jr, and J. V. Smith, Structural-electronic relationships in inorganic solids: powder neutron diffraction studies of the rutile and anatase polymorphs of titanium dioxide at 15 and 295 k, *Journal of the American Chemical Society* **109**, 3639 (1987).
- [5] H. Karzel, W. Potzel, M. Köfferlein, W. Schiessl, M. Steiner, U. Hiller, G. Kalvius, D. Mitchell, T. Das, P. Blaha, *et al.*, Lattice dynamics and hyperfine interactions in zno and znse at high external pressures, *Physical Review B* **53**, 11425 (1996).
- [6] P. Woodward, A. Sleight, and T. Vogt, Structure refinement of triclinic tungsten trioxide, *Journal of Physics and Chemistry of Solids* **56**, 1305 (1995).
- [7] W. Wang, P. J. Strohbeen, D. Lee, C. Zhou, J. K. Kawasaki, K.-S. Choi, M. Liu, and G. Galli, The role of surface oxygen vacancies in bivo4, *Chemistry of Materials* **32**, 2899 (2020).
- [8] L. Bartel and B. Morosin, Exchange striction in nio, *Physical Review B* **3**, 1039 (1971).
- [9] M. Carey, F. Spada, A. Berkowitz, W. Cao, and G. Thomas, Preparation and structural characterization of sputtered coo, nio, and ni0. 5co0. 5o thin epitaxial films, *Journal of materials research* **6**, 2680 (1991).
- [10] C. Barrett and E. Evans, Solid solubility and lattice parameter of nio-mno, *Journal of the American Ceramic Society* **47**, 533 (1964), <https://ceramics.onlinelibrary.wiley.com/doi/pdf/10.1111/j.1151-2916.1964.tb13806.x>.
- [11] P. De Sousa, A. Gouveia, J. Sczancoski, I. Nogueira, E. Longo, M. San-Miguel, and L. Cavalcante, Electronic structure, optical and sonophotocatalytic properties of spindle-like cawo4 microcrystals synthesized by the sonochemical method, *Journal of Alloys and Compounds* **855**, 157377 (2021).
- [12] W. Smith and A. Hobson, The structure of cobalt oxide, co3o4, *Acta Crystallographica Section*

B: Structural Crystallography and Crystal Chemistry **29**, 362 (1973).

- [13] W. Chen, G. Miceli, G.-M. Rignanese, and A. Pasquarello, Nonempirical dielectric-dependent hybrid functional with range separation for semiconductors and insulators, Physical Review Materials **2**, 073803 (2018).
- [14] M. Engel, H. Miranda, L. Chaput, A. Togo, C. Verdi, M. Marsman, and G. Kresse, Zero-point renormalization of the band gap of semiconductors and insulators using the projector augmented wave method, Physical Review B **106**, 094316 (2022).
- [15] Y. Ping, D. Rocca, and G. Galli, Optical properties of tungsten trioxide from first-principles calculations, Physical Review B—Condensed Matter and Materials Physics **87**, 165203 (2013).
- [16] J. Wiktor, I. Reshetnyak, F. Ambrosio, and A. Pasquarello, Comprehensive modeling of the band gap and absorption spectrum of bivo 4, Physical review materials **1**, 022401 (2017).
- [17] M. S. Abdallah and A. Pasquarello, Quasiparticle self-consistent gw with effective vertex corrections in the polarizability and the self-energy applied to mno, feo, coo, and nio, Physical Review B **110**, 155105 (2024).
- [18] R. H. French, Electronic band structure of al2o3, with comparison to alon and ain, Journal of the American Ceramic Society **73**, 477 (1990).
- [19] R. Whited, C. J. Flaten, and W. Walker, Exciton thermoreflectance of mgo and cao, Solid State Communications **13**, 1903 (1973).
- [20] K. Irmscher, M. Naumann, M. Pietsch, Z. Galazka, R. Uecker, T. Schulz, R. Schewski, M. Albrecht, and R. Fornari, On the nature and temperature dependence of the fundamental band gap of in2o3, physica status solidi (a) **211**, 54 (2014).
- [21] M. Feneberg, J. Nixdorf, C. Lidig, R. Goldhahn, Z. Galazka, O. Bierwagen, and J. S. Speck, Many-electron effects on the dielectric function of cubic in 2 o 3: Effective electron mass, band nonparabolicity, band gap renormalization, and burstein-moss shift, Physical Review B **93**, 045203 (2016).
- [22] Y. Tezuka, S. Shin, T. Ishii, T. Ejima, S. Suzuki, and S. Sato, Photoemission and bremsstrahlung isochromat spectroscopy studies of tio2 (rutile) and srtio3, Journal of the Physical Society of Japan **63**, 347 (1994).
- [23] A. Mang, K. Reimann, *et al.*, Band gaps, crystal-field splitting, spin-orbit coupling, and exciton binding energies in zno under hydrostatic pressure, Solid state communications **94**, 251 (1995).

- [24] J. Meyer, M. Kröger, S. Hamwi, F. Gnam, T. Riedl, W. Kowalsky, and A. Kahn, Charge generation layers comprising transition metal-oxide/organic interfaces: Electronic structure and charge generation mechanism, *Applied Physics Letters* **96** (2010).
- [25] J. K. Cooper, S. Gul, F. M. Toma, L. Chen, Y.-S. Liu, J. Guo, J. W. Ager, J. Yano, and I. D. Sharp, Indirect bandgap and optical properties of monoclinic bismuth vanadate, *The Journal of Physical Chemistry C* **119**, 2969 (2015).
- [26] G. Sawatzky and J. Allen, Magnitude and origin of the band gap in nio, *Physical review letters* **53**, 2339 (1984).
- [27] M. Gvishi and D. Tannhauser, Hall mobility and defect structure in undoped and cr or ti-doped coo at high temperature, *Journal of Physics and Chemistry of Solids* **33**, 893 (1972).
- [28] E. Kurmaev, R. Wilks, A. Moewes, L. Finkelstein, S. Shamin, and J. Kuneš, Oxygen x-ray emission and absorption spectra as a probe of the electronic structure of strongly correlated oxides, *Physical Review B—Condensed Matter and Materials Physics* **77**, 165127 (2008).
- [29] R. Grasser, E. Pitt, A. Scharmann, and G. Zimmerer, Optical properties of cawo4 and camoo4 crystals in the 4 to 25 ev region, *physica Status Solidi (b)* **69**, 359 (1975).
- [30] Y. Zhang, N. Holzwarth, and R. Williams, Electronic band structures of the scheelite materials camoo 4, cawo 4, pbmoo 4, and pbwo 4, *Physical Review B* **57**, 12738 (1998).
- [31] V. Shinde, S. Mahadik, T. Gujar, and C. Lokhande, Supercapacitive cobalt oxide (co<sub>3</sub>o<sub>4</sub>) thin films by spray pyrolysis, *Applied Surface Science* **252**, 7487 (2006).